ORNL/TM-2023/3029

Testing of an Optical Fiber–Based Gamma Thermometer in the High Flux Isotope Reactor Gamma Irradiation Facility

Anthony Birri
Daniel C. Sweeney
Nick Russell
Krystin Stiefel
Michael Crowell
Michael Fuller
Ed Triplett Jr.
Christian M. Petrie

OAK RIDGE National Laboratory

ORNL IS MANAGED BY UT-BATTELLE LLC FOR THE US DEPARTMENT OF ENERGY

ORNL/TM-2023/3029

Nuclear Energy and Fuel Cycle Division

TESTING OF AN OPTICAL FIBER–BASED GAMMA THERMOMETER IN THE HIGH FLUX ISOTOPE REACTOR GAMMA IRRADIATION FACILITY

Anthony Birri
Daniel C. Sweeney
Nick Russell
Krystin Stiefel
Michael Crowell
Michael Fuller
Ed Triplett Jr.
Christian M. Petrie

Milestone M3CT-23OR0703082
August 2023

Prepared by
OAK RIDGE NATIONAL LABORATORY
Oak Ridge, TN 37831
managed by
UT-Battelle LLC
for the
US DEPARTMENT OF ENERGY
under contract DE-AC05-00OR22725

CONTENTS

ACKNOWLEDGMENTS

This work is funded by the US Department of Energy's Advanced Sensors and Instrumentation Program and a Nuclear Science User Facilities Rapid Turnaround Experiment Award. The authors would like to acknowledge Kurt Smith, Shay Chapel, Heath McCartney, Bob Sitterson, David Bryant, and Doug Kyle for their support in the areas of mechanical design, drafting, assembly, and welding of the experiment described in this report. The authors would also like to acknowledge Dillon Sprague, Nicholas Smith, and Scott Brinkmeier for operations associated with the gamma thermometer on the day of experimentation. Logistical decisions, regarding experimental planning and irradiation details, were informed by consultation with Richard Howard and N. Dianne Bull Ezell. Finally, this work would not have been possible without the guidance and expertise of Dr. Thomas Blue at The Ohio State University.

ABBREVIATIONS

OBR	optical backscatter reflectometer
OFBGT	optical fiber–based gamma thermometer
HFIR	High Flux Isotope Reactor
GIF	Gamma Irradiation Facility
BWR	boiling water reactor
LPRM	local power range monitor
TIP	traverse in-core probe
GT	gamma thermometer
OFDR	optical frequency domain reflectometry

SUMMARY

This report describes the design, thermal modeling, and gamma irradiation testing of an optical fiber–based gamma thermometer (OFBGT), which was irradiated in the High Flux Isotope Reactor (HFIR) Gamma Irradiation Facility (GIF). OFBGTs are a promising technology for application in nuclear reactors because they can provide a distributed measurement of gamma ray heating rate, unlike thermocouple-based gamma thermometers, which are fixed in-core sensors that can be used in boiling water reactors to calibrate local power range monitors. OFBGTs measure gamma ray heating rate by measuring the temperature difference between a pair of optical fibers; one fiber is in thermal contact with a heat sink (usually the reactor coolant), and the other is in thermal contact with a thermally isolated mass. The device can be calibrated with a heating wire within the thermal mass. The OFBGT that was designed and fabricated at Oak Ridge National Laboratory can measure distributed gamma ray heating rate over an effective measurement length of 61 cm, and the outer diameter of the sensor is 12.7 mm, giving the prototypical sensor design a relatively small footprint. The sensor housing is backfilled with Ar to ensure a well-predicted thermal response that is not affected by humidity or chemical interactions during operation. For calibration, the sensor design uses a Ni–Cr wire, which can be supplied with currents from 0 to 1 A to capture the wide range of potential gamma ray heating rates expected in HFIR's spent fuel elements.

The OFBGT was thermally modeled analytically and numerically; both models account for temperature-dependent thermal conductivities of the materials and show good agreement. The thermal response of the sensor inside spent HFIR fuel elements was simulated for times up to 1 year after discharge of the fuel element. Out-of-pile open-air tests indicated that the steady-state response of the sensor matches modeled results within experimental uncertainty. Calibration tests were performed using electrical heating in the HFIR spent fuel pool, above the fuel elements, to establish a relationship between the difference in spectral shift measured by optical fibers located inside and outside the OFBGT and the applied electrical heating. Subsequently, the OFBGT was placed within the the spent fuel element from HFIR cycle 501 to measure the spatial profile of the gamma heating rates. Results showed good agreement between the theoretical and measured gamma dose rate profiles, with maximum deviations of ~10% or less.

1. INTRODUCTION

Monitoring of the volumetric power distribution in a nuclear reactor is crucial for safe and reliable operations. The power distribution may become perturbed over the life of the core because of a range of possible reactor kinetic conditions [1–7]. It is important that these perturbations be characterized so that appropriate actions may be taken to stabilize the power distribution. In general, the volumetric power distribution is monitored with in situ and ex situ sensors that detect neutron and/or gamma ray radiation. These sensors include fission chambers, self-powered neutron detectors, self-powered gamma detectors, ion chambers, and gamma thermometers (GTs) [8–14]. Thermocouple data can also be used to infer aspects of the volumetric power distribution [15]. A variety of algorithms exist to solve the inverse (i.e., a volumetric power distribution from in situ and ex situ sensor responses) [16–18].

In boiling water reactors (BWRs) specifically, the volumetric power distribution is typically monitored by local power range monitors (LPRMs), which is an industry-specific name for an array of fission chambers. Over time, LPRMs lose sensitivity because of burnup of the fissionable material and must be recalibrated. Currently, LPRMs are calibrated with traversing in-core probes (TIPs). TIPs are also fission chambers, so they need to be inserted into the core for calibration and removed after calibration to avoid burnup within the TIPs. There can be approximately 170 LPRMs that require recalibration in a BWR [19], and

positioning a TIP next to each LPRM involves a complex process of passing the TIP through numerous valves designed to prevent the release of radioactive material into the environment. Also, even with these valves in place, a release of radioactive material is still possible.

A way to prevent the release of radioactive materials from the reactor vessel is to establish a permanent system of radiation-tolerant sensors for LPRM calibration. Ideally, these sensors could be calibrated without removing and reinserting them into the core. GTs have been developed for this purpose. GTs are designed to be radiation damage–insensitive detectors that measure local gamma ray heating rates. The gamma ray heating rate measurement in a GT can be used to recalibrate an adjacent LPRM, assuming that the relationship between heating rate and power is known for the core configuration. Furthermore, a system of state-of-the-art GTs for LPRM calibration could be improved by making them optical fiber based. Unlike a GT, which is a point sensor, an optical fiber–based gamma thermometer (OFBGTs) can be constructed to be a distributed sensor: that is, it can acquire a distributed temperature measurement along the length of an optical fiber using optical frequency domain reflectometry (OFDR), or perhaps using a cascade of distributed fiber Bragg gratings interrogated with a more standard spectrometry technique. One could therefore calibrate all of the LPRMs along the length of an instrument tube in a BWR with one OFBGT instead of multiple GTs, thereby reducing the total cabling involved and decreasing the footprint. It has been shown that OFBGTs could also be used for direct inferencing of the core power distribution, potentially at a high fidelity because of their ability to acquire significantly more data points than an array of point sensors [20].

This report covers the design, development, out-of-pile testing, calibration, and gamma irradiation of an OFBGT to measure the axial distribution of gamma ray heating rates in spent fuel elements. The OFBGT was tested in the High Flux Isotope Reactor (HFIR) spent fuel pool to provide an environment that does not include the effects of neutron radiation. This work complements other experimental OFBGT testing that has been performed in the Ohio State University reactor and the Texas A&M Testing, Research, Isotopes, General Atomics reactor involving slightly varying OFBGT designs and irradiation conditions [21, 22]. The combined output of these tests will help inform sensor optimization and separate the effects of neutron and gamma radiation on sensor performance. Furthermore, the present work has a synergy with concurrent development of OFBGTs and data processing algorithms that can be used to infer reactor power distributions based on the response of an OFBGT array.

2. PRINCIPLES OF OPERATION

A basic diagram of a GT is shown in Fig. 1. In its most basic depiction, a GT can be considered as a three-region system comprising a thermal mass, an outer sheath, and a gas gap between the thermal mass and outer sheath. In this depiction, the thermal mass is a solid cylinder and the outer sheath is a tube. Its cylindrical geometry allows the GT to be placed in line with fuel assemblies in a reactor core and to monitor the entire length of the reactor core. Gamma rays interact with and thereby deposit heat energy in the thermal mass. Neutrons also interact with the thermal mass, but materials may be chosen such that the neutrons' contribution to the total heating rate is significantly smaller than that of gamma rays [21]. Gamma rays (and to a lesser extent neutrons) also deposit energy in the outer sheath and gas gap. However, one can ignore the energy contributions to these two regions because of the low density of the gas gap and the thermal contact between the outer sheath and the ambient cooling environment.

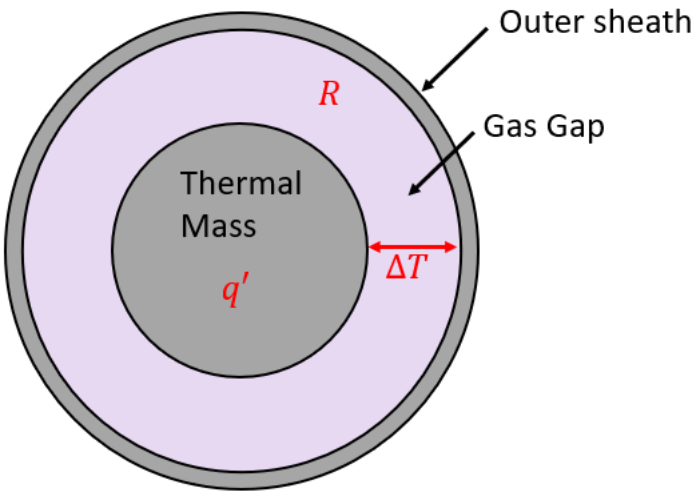

Figure 1. Basic depiction of a GT.

The volumetric heating in the thermal mass can be expressed as a linear heating rate, q', by integrating over the cross-sectional area at a given axial location along the GT. The gas gap, due to its low thermal conductivity, is the region with the most significant thermal resistance, given by R. The q' drives a ΔT across the R of the gas gap. Because the gas gap has the dominant thermal resistance out of the three regions, the radial temperature differences across the thermal mass and outer sheath can be neglected (to a first order). The three aforementioned terms are related by

$$\Delta T = q'R \, . \tag{1}$$

Whereas Fig. 1 depicts a GT that could be either thermocouple or optical fiber based and ignores geometrical nuances and finer details, Fig. 2 shows a more detailed depiction of an OFBGT. The OFBGT follows the basic operating principles and design of the GT in Fig. 1, with ΔT as a function of axial length ($\Delta T(z)$) measured with a pair of optical fiber temperature sensors instead of with a pair of thermocouples. The optical fibers are configured such that one optical fiber measures the axially distributed temperature in the thermal mass, and one optical fiber measures the axially distributed temperature of the outer sheath; $\Delta T(z)$ is the axially dependent difference in temperature between these fibers. In most thermocouple- or optical fiber–based GT designs that exist in literature, a single thermal mass is associated with a single measurement of ΔT [23–28, 19]. In the case of the OFBGT described herein, a single thermal mass is capable of providing many ΔT measurements (hence $\Delta T(z)$) along its axial length.

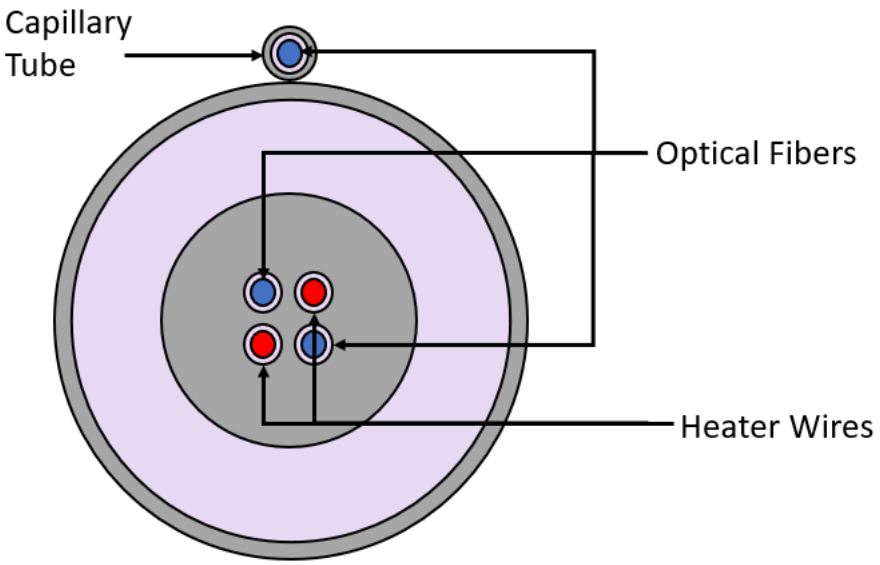

Figure 2. Depiction of an OFBGT.

Two optical fiber sensors run through two holes in the thermal mass, allowing for redundancy in the measurement of $\Delta T(z)$. The optical fibers can be interrogated over their lengths using OFDR to measure their temperatures. A single heating wire runs down one (the third) of the remaining two holes in the thermal mass, is bent 180°, and returns through the final (fourth) hole in the thermal mass to a power supply to complete an electrical circuit. The purpose of the heating wire is for calibration of the OFBGT. If a known power is applied to the heating wire, and the heating wire's length is known, then the q' the wire generates can be determined. By varying the joule heating of the wire, a relationship can be developed between q' and ΔT. Then, when the OFBGT is heated by gamma rays, the measured $\Delta T(z)$ can be related to a corresponding gamma ray–induced $q'(z)$ using the previously determined calibration. Note that if a significant heat flux is expected in the axial direction, then the modulation of $\Delta T(z)$ may be able to be addressed when converting from $\Delta T(z)$ to $q'(z)$ using a modulation transfer function [29, 30].

3. EXPERIMENTAL DESIGN

A depiction of the OFBGT assembly that was used for testing in HFIR's GIF is shown in Fig. 3. Within the irradiated region, the OFBGT sits in a custom irradiation basket, which can be lowered into a spent fuel element in the spent fuel pool via the eye hooks at the top of the basket. The OFBGT is mechanically attached to the basket via a threaded connection between the bottom of the OFBGT and the inner bottom of the irradiation basket. The rigid extension tube protects lead-in wires and fibers connected to the fibers and heater wire within the OFBGT. The rigid extension tube is connected to the OFBGT via a Swagelok fitting. There is a gas intake line which is intended to feed an overpressure of Ar to the assembly throughout testing. A vacuum-rated epoxy is used to create a hermetic seal through which the lead-in fibers and wires pass between the flexible extension tube and the rigid extension tube.

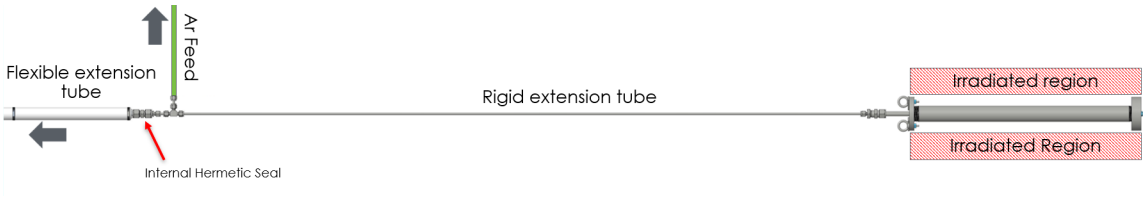

Figure 3. Assembly of the OFBGT experiment for irradiation in the HFIR spent fuel pool.

A close-up, external view of the OFBGT and the irradiation basket is shown in Fig. 4(a). Flow holes are drilled into centering disks at the top and bottom of the irradiation basket to allow for natural convective flow through the spent fuel assembly. Three tabs are welded to the top centering disk of the basket to allow the basket to sit at the appropriate axial location within the spent fuel element. On the OFBGT, both the outer sheath and capillary tube are visible. The capillary tube is tack-welded to the OFBGT via small metal strips. The bottom of the OFBGT and the capillary tube are capped using a Swagelok plug. The fittings on the OFBGT are fabricated with stainless steel 316, and the bulk metal components of both the irradiation basket and the OFBGT are fabricated with stainless steel 304. The OFBGT and custom basket are approximately 61 cm in length. The outer diameter of the OFBGT is 12.7 mm, and the outer diameter of the irradiation basket is 42.2 mm.

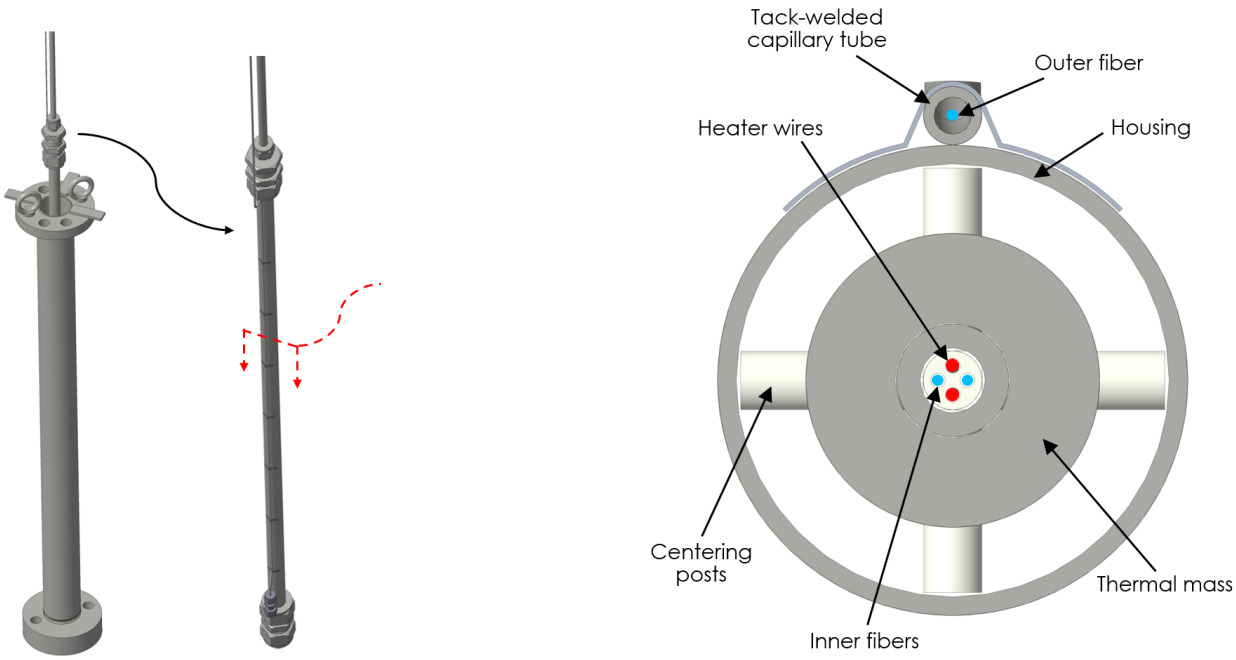

Figure 4. (a) The irradiation basket and an external view of the OFBGT, and (b) a cross-sectional view of the OFBGT.

A cross-sectional view of the OFBGT is shown in Fig. 4(b). The bulk of the thermal mass consists of two concentric stainless steel 304 tubes that are welded together to create an assembly with nominal inner and

outer diameters, thereby achieving the desired gas gap thickness and minimizing clearance between the thermal mass and the inner alumina insulators. Welding of standard-size components was preferred because it would be difficult to fabricate a custom thermal mass long enough to achieve the desired inner-to-outer-diameter ratio. The alumina insulators house the optical fibers and heating wire at the center of the thermal mass. The heating wire is a Ni–Cr alloy (80/20). The fibers are inscribed with fiber Bragg gratings to enhance the intensity of the backscattered light when interrogating the fibers with OFDR and hopefully compensate for any darkening that occurs under gamma irradiation. Along the axial length of the thermal mass, several zirconia centering posts are inserted into holes in the sides of the thermal mass to center it within the outer sheath. Zirconia was chosen for its low thermal conductivity to limit radial heat losses at these post locations.

4. THERMAL MODELING

The axially and radially dependent temperature profile of the OFBGT was analyzed as a function of time relative to the end of an operating HFIR cycle because each spent HFIR fuel element available for irradiation testing will have a different cooling time. This analysis required knowledge of the spatial dependence of the dose rate within the fuel element as a function of days since cycle end. Figure 5 shows calculated results for the maximum dose rate as a function of days since the end of a HFIR cycle as well as the normalized axial gamma heating rate profile. In this work, the normalized axially dependent gamma heating profile is approximated as a cosine function, which is motivated by the analytic mathematics discussed in the next paragraph. This dose rate information, which was provided by HFIR staff, can be converted into heating rates using the mass attenuation coefficient of the thermal mass. The experimental measurements described in this report will be helpful for validating the calculated evolution of the dose rates.

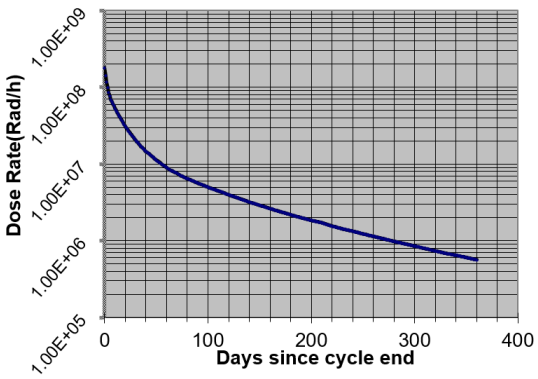

(a)

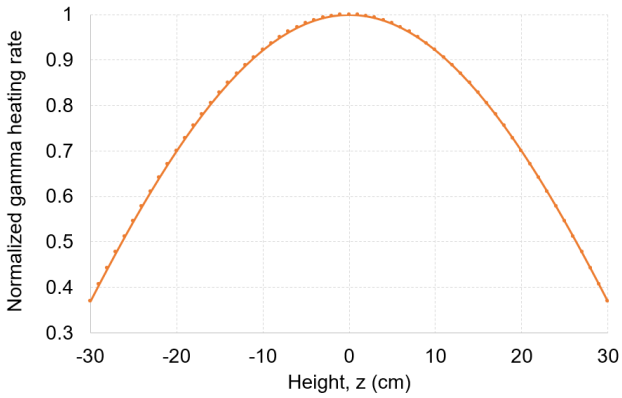

(b)

Figure 5. (a) Maximum gamma dose rate in a spent HFIR fuel element as a function of days since cycle and, and (b) the normalized axial gamma heating rate profile in a spent fuel element.

Both analytical and numerical approaches were used to generate and verify thermal models. The analytical approach, which is described in detail in Birri et al. [30], involves solving the radial coordinate heat conduction equations for a three-region, concentric cylinder geometry. The azimuthal dependence is

ignored, but the radial and axial dependencies are considered. In the axial direction, a sinusoidal function is assumed for the heat generation rate in the thermal mass. In the radial direction, the temperature profiles in the thermal mass, gas gap, and outer sheath are each described by two unique summative Bessel functions, resulting in six constants for which to solve. The solution involves simultaneous determination of these six constants in boundary conditions of the radially dependent temperature profile. Temperature-dependent thermal conductivities are considered by iteratively solving for the temperature profile for a given heating rate profile by updating the thermal conductivities in each iteration of the temperature profile until convergence is achieved. The ANSYS (version 19.0) steady-state thermal modeling package was used to verify the analytical model numerically using the same axial heat generation rate applied to the thermal mass in the analytical model. Temperature-dependent thermal conductivites were considered in the numerical model as well.

As a validating test case, the analytical and numerical models were used to generate temperature profiles at the radial center of the OFBGT 10 days after the end of the cycle. As shown in Fig. 6, the two methods generated very similar profiles with < 1% discrepancy. The axial and radial dependencies of the temperature profile generated by the analytical model are shown for 10 days after cycle end in Fig. 7.

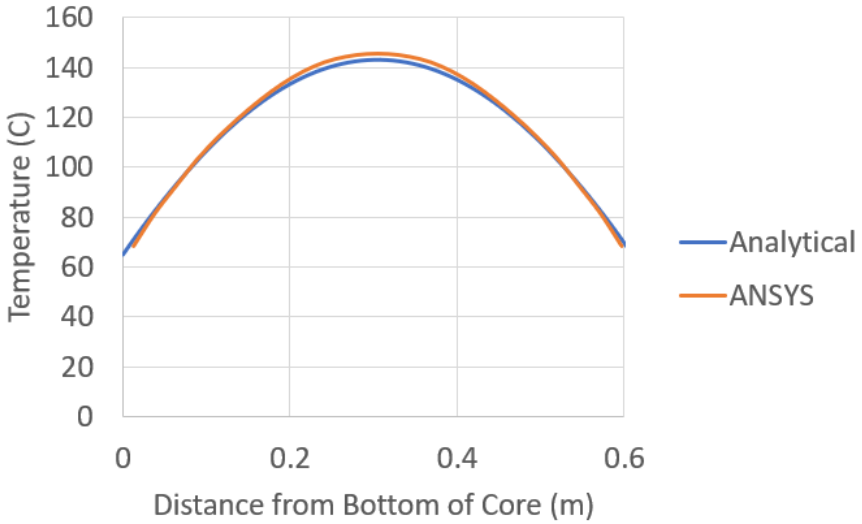

Figure 6. Comparison of the numerically and analytically calculated centerline axial temperature profiles in the OFBGT 10 days from cycle end.

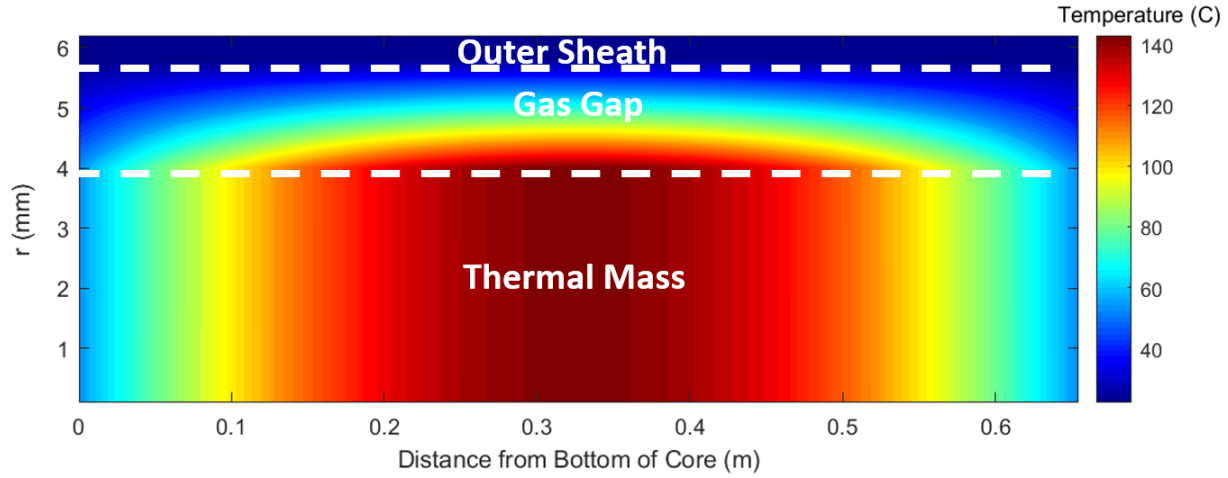

Figure 7. Temperature profile in the OFBGT 10 days after cycle end, as calculated by the analytical model.

For experimental planning purposes, it is important to consider how the peak magnitude of the temperature profile decreases as a function of time; for a given fuel element, there will come a point at which too much time has elapsed since cycle end to be able to detect a significant ΔT between the thermal mass fiber and the capillary fiber. For this reason, the maximum ΔT is plotted in Fig. 8 as a function of the time from the end of a HFIR cycle, over a period of one year. The maximum ΔT drops below 10°C a little after 100 days and 5°C after 200 days. After a year, the maximum ΔT is estimated to be 1.4°C. If one assumes an accuracy of ±1°C for OFDR, then based on Fig. 8, experimentation should only occur on fuel elements that are < 200 days from cycle end to avoid high relative uncertainty in the measurements and to ensure that a reliable axial temperature distribution can be measured.

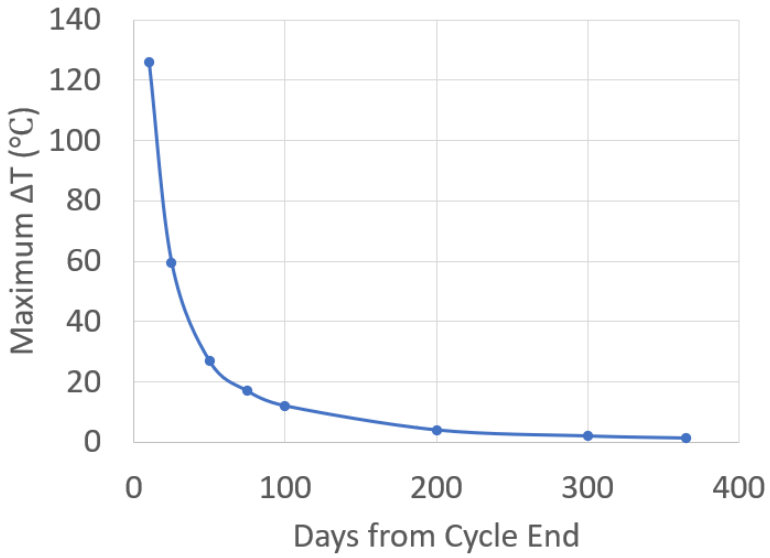

Figure 8. Maximum ΔT in the OFBGT as a function of days since cycle end.

5. OUT-OF-PILE TESTING

The OFBGT was tested out of pile to ensure the sensor was working appropriately before full assembly in preperation for in-pile testing. In these tests, the OFBGT was not evacuated, backfilled, or submerged in water. Therefore, the gas gap was composed of air, and the outer surface was cooled only by natural convection of the surrounding air. The OFBGT was electrically heated by passing a range of currents through the nichrome heating wire. The out-of-pile tests do not serve as calibration measurements because the gaseous volume within the OFBGT is intended to be Ar during operation in the HFIR spent fuel pool, and also because the heat transfer coefficient of the ambient air is low, which prolongs the time required to reach thermal equilibrium. However, these open-air tests can be used for confirmation that the OFBGT is generating ΔT measurements consistent with those determined using thermal modeling, at least for currents low enough for the sensor to be able to reach thermal equilibrium.

The results of the out-of-pile tests are shown in Fig. 9. The entire scope of the experiment is shown in Fig. 9(a), which shows that sensor responses are stable up to the temperatures expected when testing in the HFIR spent fuel pool. In Fig. 9(b), the steady-state ΔT values are plotted as a function of currents up to approximately 0.43 A and compared with the analytically modeled ΔT values, which were obtained by converting current to a linear heating rate. The modeled ΔT values agree with the sensor experimental ΔT values within the margin of experimental uncertainty.

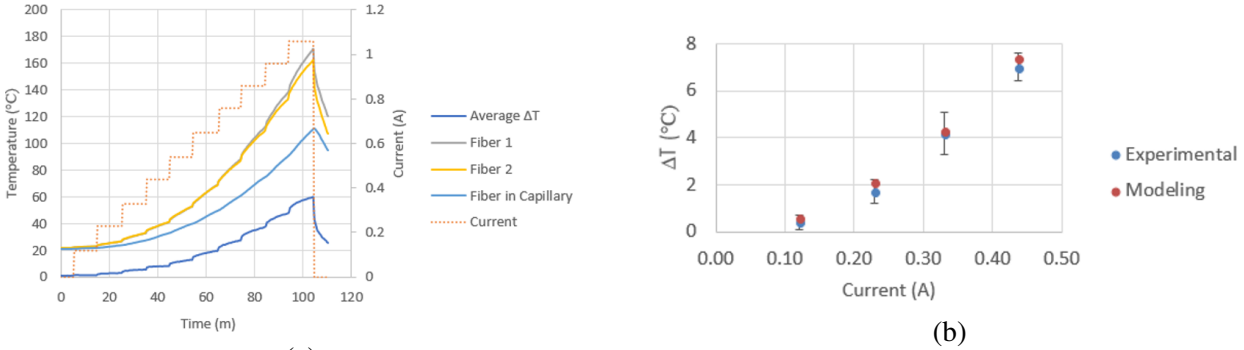

(a) (b)

Figure 9. (a) Results from out-of-pile nichrome heating test of the OFBGT in air with electrical heating at currents from 0 to 1 A, and (b) comparison of experimental and modeled ΔT values for low currents at which steady state was achieved.

6. TESTING IN THE GIF

6.1 IN-POOL CALIBRATION

Prior to insertion into the GIF pool, the OFBGT was backfilled with 20 psig of ultrapure Ar. This overpressurization was to prevent potential leakage of water into the experiment at the bottom of the pool, where the water pressure is ~10 psig. Upon arrival at HFIR, the interrogation device (Optical Backscatter Reflectometer [OBR]-4600) and the power supply (Sorensen LHP 60-18 DC power supply) were set up in a radiation buffer zone on the side of the spent fuel pool as shown in Fig. 10. The Ar feed tube was connected to an Ar gas cylinder in the buffer zone for constant pressure regulation throughout the experiment. The OFBGT was loaded into the custom basket and lowered into the pool via the eye bolts on

the top of the basket. For in-pool calibrations, the OFBGT was fully submerged in the pool but not yet lowered into a spent fuel element. Fig. 11(a) shows an image of the OFBGT within the custom basket and submerged in the pool.

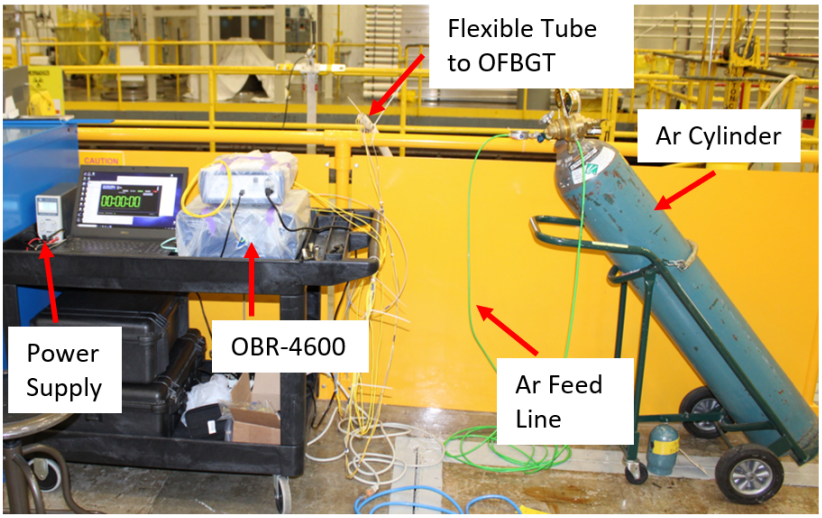

Figure 10. Setup of the OBR-4600, power supply, and gas supply equipment in the buffer area next to the GIF.

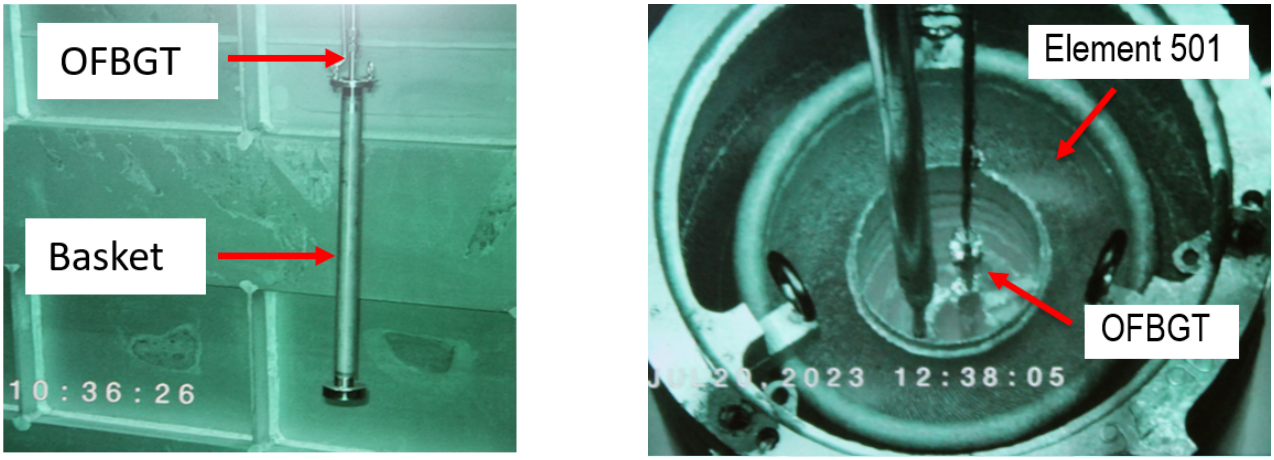

(a) (b)

Figure 11. (a) OFBGT inserted in the GIF pool and configured for electrical heating calibration tests and (b) OFBGT inserted into spent fuel element 501 for active scans during gamma ray irradiation.

The power supply was stepped up in current from 0 to 0.7 A in 0.1 A increments to calibrate the OFBGT under the ambient water-cooled, Ar-backfilled conditions. The OFBGT was allowed 20 min to reach thermal equilibrium at each step before a scan was taken with the OBR. The results of this calibration were curves that were used to convert the difference in spectral shift in a given thermal mass fiber and capillary fiber, $\Delta(\delta S)$, to a linear heating rate, q'. These curves are shown in Fig. 12 using measurements from both

of the thermal mass fibers to determine $\Delta(\delta S)$; the spatially averaged $\Delta(\delta S)$ obtained from each of the two thermal mass fibers was considered, such that the averages were taken over the thermal mass length. The reference scans for these $\Delta(\delta S)$ measurements were taken before any electrical current was applied to the OFBGT but after the OFBGT was allowed 20 min to reach thermal equilibrium in the pool. The conversion factor between δS and ΔT is approximately $\Delta T = 3\delta S/4$ for the temperature range considered in this study [31].

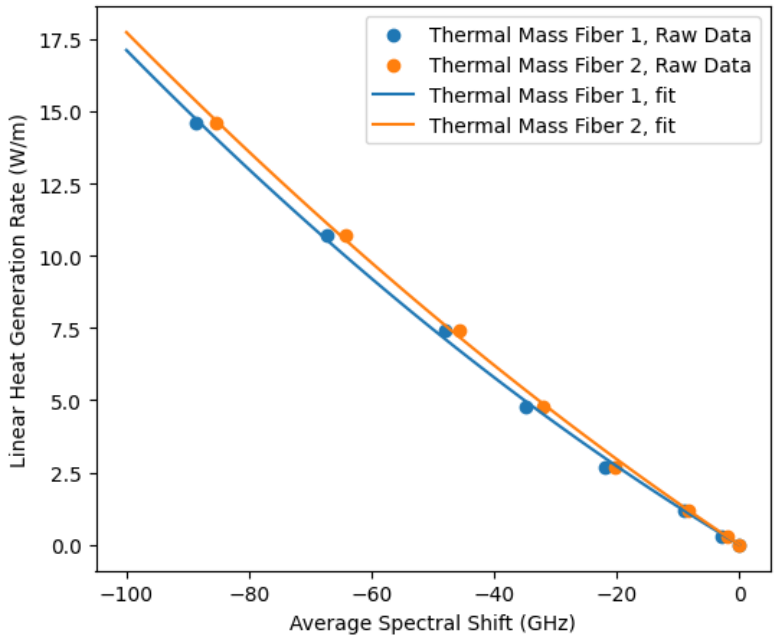

Figure 12. Calibration curves to relate $\Delta(\delta S)$ to q' obtained using both thermal mass fibers in the OFBGT.

6.2 IN-PILE TESTING

After the OFBGT was calibrated, it was allowed 20 min to reach ambient temperatures within the GIF pool. After this time passed, another reference scan was taken to act as the reference scan for active irradiation measurements. The OFBGT was then inserted into the spent fuel element from cycle 501. This cycle had ended 32 days before this gamma irradiation, which resulted in an expected peak dose rate of 20 Mrad/h based on the data shown in Fig. 5(a). These data were generated from coupled MCNP and ORIGEN simulations of a typical ~23–25 day HFIR cycle. The models used for these simulations were described in more detail in previously [32]. Four scans were taken in cycle 501 at 5 min increments. The OFBGT is shown within this element in Fig. 11(b). The $\Delta(\delta S)$ data acquired as a function of axial length along the thermal mass were converted to q' using relations in Fig. 12 and then to dose rate by dividing by the density of the thermal mass and applying appropriate conversion factors to get to units of Mrad/h.

The axially dependent measured dose rates based on both thermal mass fibers are shown in Fig. 13. These dose rate profiles are based on the different calibration curves for each thermal mass fiber shown in 12. Note 0.0 m represents the top of the thermal mass, and distances greater than 0.0 are within the thermal

mass. In general, both curves agree reasonably well with the theoretical gamma dose rate axial distribution, within ~10%. The agreement is stronger for thermal mass fiber 2. There was some detectable hysteresis in the response of the thermal mass fibers (not shown) before and after calibration. This suggests that there may be some strain coupling between the fibers and the thermal mass insulator. This could be mitigated in an optimized design by removal of the acrylate coating on the fibers, which notably improved OFBGT performance in studies at The Ohio State University [21]. Based on the discrepancy between thermal mass fiber 1 and thermal mass fiber 2 in Fig. 13, this strain coupling could be affecting the fibers differently; this also could explain the discrepancy in calibration curves in Fig. 12.

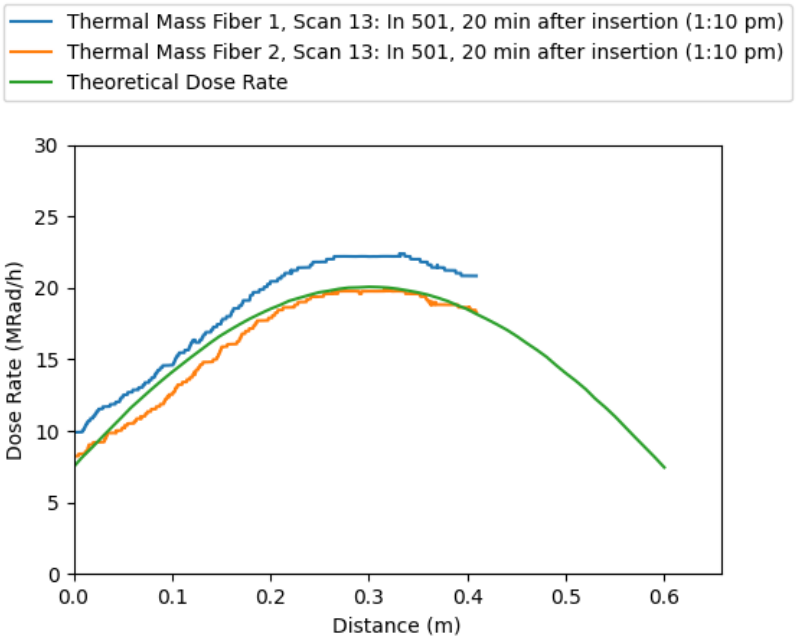

Figure 13. Gamma ray dose rate distributions measured by the OFBGT, using both thermal mass fibers, compared with the theoretical distribution.

Another aspect of Fig. 13 to note is the slight difference in shape between the experimental versus theoretical profiles. This is particularly noticeable in thermal mass fiber 2, which peaks at a similar magnitude as the theoretical curve but follows a slightly different profile moving toward the top (toward a distance of 0 m) fo the OFBGT. This was somewhat anticipated because the thermal mass is constructed of stainless steel, which has a relatively high thermal conductivity that can result in significant axial heat transfer and modulate the axial temperature profile compared with the gamma ray energy deposition profile [20]. Regardless, the profile modulation appears to be slight and could be minimized with use of lower thermal conductivity materials. However, one trade-off of choosing lower thermal conductivity materials is that they generally have low densities; stainless steel offers the advantage of a higher-sensitivity OFBGT because higher heat generation rates would be expected per unit volume of the thermal mass material.

7. CONCLUSION

An OFBGT designed to measure spatial gamma ray dose rate profiles was designed, modeled, fabricated, tested out of pile, and tested in the spent fuel element from HFIR cycle 501 in the GIF. The analytical and numerical thermal models produce consistent values for the measured ΔT, and the analytical model was experimentally validated in the out-of-pile, electrically heated tests. The OFBGT was calibrated in the GIF pool to establish a relationship between energy deposition rate and spectral shift difference between fibers thermally insulated in a thermal mass and a fiber thermally coupled to the ambient water environment. The OFBGT showed reasonable agreement with the theoretical gamma ray dose rate profile in the spent fuel element. In general, the findings of this report suggest that the OFBGT is a feasible technology for measuring extremely high gamma ray dose rate spatial distributions, such as for spent fuel gamma ray profile characterization. The next step is to evaluate whether this could be extended to nuclear reactor applications, such as in-situ flux shape monitoring.

8. REFERENCES

[1] B. Mercier, Z. Ziliang, C. Liyi, and S. Nuoya, "Modeling and Control of Xenon Oscillations in Thermal Neutron Reactors," *EPJ Nuclear Sci. Technol.*, vol. 6, p. 48, 2020.

[2] A. Chakraborty, M. P. S. Fernando, and A. S. Pradhan, "Performance of Flux Mapping System During Spatial Xenon Induced Oscillations in PHWRs," in *Proceedings of the 7th International Conference on Advances in Energy Research* (M. Bose and A. Modi, eds.), (Singapore), pp. 1559–1570, Springer Singapore, 2021.

[3] P. Mala, H. Ferroukhi, A. L. Vasiliev, M. Seidl, and D. Janin, "Bowing Effects on Power and Burn-Up Distributions for Simplified Full PWR and BWR Cores," in *International Conference on Mathematics and Computational Methods Applied to Nuclear Science and Engineering*, (Jeju, Korea), 2017.

[4] J. Li, "Monte Carlo Investigation of the UK's First EPR Nuclear Reactor Startup Core Using Serpent," *Energies*, vol. 13, no. 19, 2020.

[5] A. Dandi, M. Lee, and M. H. Kim, "Feasibility of Combinational Burnable Poison Pins for 24-month Cycle PWR Reload Core," *Nuclear Engineering and Technology*, vol. 52, no. 2, pp. 238–247, 2020.

[6] F. M. Zadeh, S. Etienne, R. Chambon, G. Marleau, and A. Teyssedou, "Effect of 3-D Moderator Flow Configurations on the Reactivity of CANDU Nuclear Reactors," *Annals of Nuclear Energy*, vol. 99, pp. 136–150, 2017.

[7] M. Torabi, A. Lashkari, S. F. Masoudi, and S. Bagheri, "Neutronic Analysis of Control Rod Effect on Safety Parameters in Tehran Research Reactor," *Nuclear Engineering and Technology*, vol. 50, no. 7, pp. 1017–1023, 2018.

[8] Y. Nishizawa, "Reactor Power Control Apparatus," 1982. US Patent 4,333,797A.

[9] A. J. I. Jr., "Method and Apparatus for Continuous On-Line Synthesis of Power Distribution in a Nuclear Reactor Core," 1987. US Patent 4,637,910A.

[10] A. J. I. Jr. and L. R. Grobmyer, "Method and Apparatus for Continuous On-Line Synthesis of Power Distribution in a Nuclear Reactor Core," 1988. US Patent 4,774,049A.

[11] A. J. I. Jr. and L. R. Grobmyer, "A Method and Apparatus for Continuous Nuclear Power Distribution Synthesis," 1989. EP0323280A2.

[12] A. J. I. Jr. and L. R. Grobmyer, "Continuous, Online Nuclear Power Distribution Synthesis System and Method," 1989. US Patent 4,839,134A.

[13] M. D. Heibel, "Method and a System for Accurately Calculating PWR Power from Excore Detector Currents Corrected for Changes in 3-D Power Distribution and Coolant Density," 1996. US Patent 5,490,184A.

[14] K. Hirukawa, S. Sakurai, and T. Naka, "Nuclear Reactor Power Distribution Monitoring System and Method Including Nuclear Reactor Instrumentation System," 2001. US Patent 6,236,698B1.

[15] A. J. I. Jr., "Axial Power Distribution Monitor and Display Using Outputs from Ex-Core Detectors and Thermocouples," 1988. US Patent 4,774,050.

[16] M. G. Park and H. C. Shin, "Reactor Power Shape Synthesis Using Group Method of Data Handling," *Annals of Nuclear Energy*, vol. 72, pp. 467–470, 2014.

[17] I. Ramezani and M. B. Ghofrani, "Reconstruction of Neutron Flux Distribution by Nodal Synthesis Method Using Online In-Core Neutron Detector Readings," *Progress in Nuclear Energy*, vol. 131, p. 103574, 2021.

[18] A. Birri, D. C. Sweeney, and N. D. B. Ezell, "Simulating Self-Powered Neutron Detector Responses to Infer Burnup-Induced Power Distribution Perturbations in Next-Generation Light Water Reactors," *Progress in Nuclear Energy*, vol. 153, p. 104437, 2022.

[19] G. P. Koster, H. Xia, and B. K. Lee, "Optical Gamma Thermometer," tech. rep., GE Global Research, Niskayuna, New York (United States), 2013.

[20] A. Birri and T. E. Blue, "Methodology for Inferring Reactor Core Power Distribution from an Optical Fiber Based Gamma Thermometer Array," *Progress in Nuclear Energy*, vol. 130, p. 103552, 2020.

[21] A. Birri, *The Development of an Optical Fiber Based Gamma Thermometer*. PhD thesis, The Ohio State University, 2021.

[22] J. T. Gates, *High Precision Sensing of TRIGA Operational Characteristics Using Optical Fiber-Based Gamma Thermometers*. PhD thesis, Texas AM University, 2022.

[23] G. Apelqvist, T. Andersson, L. Magnusson, and K. Romslo, "Radcal Gamma Thermometers—Performance Experience from Swedish Light Water Reactors," in *In core instrumentation and reactor assessment*, 1989.

[24] K. Hirukawa, "In-Core Fixed Nuclear Instrumentation System and Power Distribution Monitoring System," June 18 2002. US Patent 6,408,041.

[25] K. Romslo and P. Moen, "Radcal Gamma Thermometer: A Promising Device for Accurate Local Fuel Power Measurements in Light Water Reactors," *NEA Specialists Mtg. on In-Core Instrumentation and Reactor Assessment*, pp. 7–10, 1984.

[26] F. Loisy, M. Huver, and M. Janvier, "Technology and Use of Gamma Thermometers," in *In core instrumentation and reactor assessment*, 1989.

[27] L. C. Wimpee, M. A. Ross, T. J. O'neil, and E. M. D. Chu, "Fixed In-Core Calibration Devices for BWR Flux Monitors," May 14 1991. US Patent 5,015,434.

[28] C. Martin, "Gamma Thermometer System for LPRM Calibration and Power Shape Monitoring," *Licensing Topical Report, GE Nuclear Energy, NEDO-33197, Revision 0*, 2005.

[29] R. K. Palmer and T. E. Blue, "Modulation Transfer Function for Distributed Temperature Measurements Using an Optical Fiber Sensor System," *IEEE Sensors Journal*, vol. 18, no. 5, pp. 1911–1918, 2018.

[30] A. Birri, C. M. Petrie, and T. E. Blue, "Analytic Thermal Model of an Optical Fiber Based Gamma Thermometer and its Application in a University Research Reactor," *IEEE Sensors Journal*, vol. 20, no. 13, pp. 7060–7068, 2020.

[31] J. T. Jones, D. C. Sweeney, A. Birri, C. M. Petrie, and T. E. Blue, "Calibration of distributed temperature sensors using commercially available smf-28 optical fiber from 22ř c to 1000ř c," *IEEE Sensors Journal*, vol. 22, no. 5, pp. 4144–4151, 2022.

[32] N. Xoubi and R. Primm III, "Modeling of the high flux isotope reactor cycle 400," tech. rep., Oak Ridge National Laboratory, Oak Ridge, Tennessee (United States).